ORIGINAL PAPER

Hydrogeochemical characterization and geochemical modeling for the evaluation of groundwater quality and health risk assessment in the Varuna River basin, India

Sangita Dey · N. Janardhana Raju · Wolfgang Gossel · R. K. Mall

Abstract This study focuses on determining significant controlling factors of chemical consequences, inverse geochemical modeling, water quality, and human health risk in the Varuna River basin of India. The study interprets that according to pH, total dissolved solids, and total hardness, the maximum number of groundwater samples are alkaline, fresh, and have substantial hardness. The abundance of major ions follows a pattern: $Na > Ca > Mg > K$, and $HCO_3 > Cl > SO_4 > NO_3 > F$. Piper diagram shows that $Ca–Mg–HCO_3$ facies are predominant during both seasons. Na-normalized molar ratios of HCO_3/Na, Mg/Na, and Ca/Na are 0.62, 0.95, and 1.82 (pre-monsoon) and 0.69, 0.91, and 1.71 (post-monsoon), respectively, elucidating the coupled silicate and carbonate weathering (dolomite dissolution) sources. The Na/Cl molar ratio is 5.3 (pre-monsoon) and 3.2 (post-monsoon), indicating silicate alteration as the primary process rather than halite dissolution. The chloro-alkaline indices confirm the presence of reverse ion- exchange. Geochemical modeling using PHREEQC identifies the formation of secondary kaolinite minerals. The inverse geochemical modeling categorizes the groundwaters along the flow path from recharge area waters (Group I: $Na–HCO_3–Cl$), transitional area waters (Group II: $Na–Ca–HCO_3$), and discharge area waters (Group III: $Na–Mg–HCO_3$). The model demonstrates the prepotency of water–rock interactions in pre-monsoon justified by the precipitation of Chalcedony and Ca-montmorillonite. The mixing analysis shows that in the alluvial plains, groundwater mixing is a significant hydrogeochemical process that affects groundwater quality. The Entropy Water Quality Index ranks 45% (pre-monsoon) and 50% (post-monsoon) of samples as an excellent category. However, the non-carcinogenic health risk assessment shows that children are more susceptible to fluoride and nitrate contamination.

Keywords Hydrogeochemical processes · Entropy Water Quality Index (EWQI) · Inverse modelling · Mixing · PHREEQC · Health risk assessment

S. Dey · R. K. Mall (✉)
DST-Mahamana Centre of Excellence in Climate Change Research, Institute of Environment and Sustainable Development, Banaras Hindu University, Varanasi 221005, India
e-mail: rkmall@bhu.ac.in

N. J. Raju
School of Environmental Sciences, Jawaharlal Nehru University, New Delhi 110067, India

W. Gossel
Institute for Applied Geology, Martin Luther University, Halle (Saale), Germany

🖄 Springer

Introduction

In recent years, many developing countries have been more concerned with preserving and sustaining groundwater resources to avoid significant public demand and health issues. However, it is arduous to gain congruence between humans, resources, and the environment (Li & Wu, 2019). Groundwater contributes roughly 62% of irrigation in India, 85% of rural water supply, and 45% of urban water supply. A hike in annual groundwater extraction was noticed from 231bcm (2004) to 245bcm (2020) (CGWB, 2021). Subsequently, easy and uncontrolled access to groundwater in India inevitably introduces waterborne health complications (UNICEF/WHO, 2004). The elemental composition of groundwater significantly impacts the severity of the detrimental consequences. Generally, the groundwater chemical components are primarily the result of subsurface geochemical processes within the underlying geology. The ability to identify the major and minor ion compositions in groundwater and recognize underlying processes is thus highly required to understand the evolution of recharge and discharge areas, flow paths, and quality assurance.

Several approaches have been used worldwide over the decades to assess groundwater hydrogeochemistry and quality along with the risk assessment, including the use of stoichiometric relations (graphical approach), multivariate statistical techniques, geochemical modeling, water quality index, etc. (Amiri et al., 2014; Barzegar et al., 2019; Jalali, 2010; Raju et al., 2012; Senthilkumar & Elango, 2013; Sharif et al., 2008; Tong et al., 2021; Zhang et al., 2020; Jandu et al., 2021). Moreover, various researchers have identified inverse geochemical modeling as a practical tool to evaluate the potential reactions and reactants in hydrochemical processes along the flow path, exemplify water origins, and track the contaminant sources (Zhang et al., 2020). Appelo (1994) proposed a one-dimensional model to predict the complicated interactions of transport and mineral and ion exchange equilibrium in an aquifer system using PHREEQE. Subsequently, the implementation of different computer algorithms (e.g., NETPATH, PHREEQC, etc.) was also frequently applied for modeling hydrogeochemical reactions along the flow

path in other watersheds over the years (Dai et al., 2006; Sharif et al., 2008; Zhang et al., 2020).

The Water Quality Index (WQI) is a traditional approximation method that has been consistently used in the qualitative evaluation of groundwater resources (Horton, 1965). It was later innovated as weighted arithmetic mean WQI for generating acceptability classes for drinking water (Brown et al., 1970). The plausible approach of EWQI (Entropy Water Quality Index) is a promising quality evaluation method as it ignores subjective approaches and involves statistical analyses. Entropy measures the extent of uncertainty associated with randomized hydrological processes. Interestingly, by quantifying observations and minimizing uncertainty, this comprehensive analysis encompasses the information content of a data set and classifies water quality in explicit categorical ranges (Amiri et al., 2014). A substantial urgency for constructing a quantitative methodology can efficiently draw contaminant severity like fluoride and nitrate contamination which have adverse quality issues on human health. Hence, the United States Environmental Protection Agency (USEPA, 2022) proposed a perceptible risk assessment methodology for human health. The procedure is efficiently used worldwide in fluoride and nitrate risk assessment (Madhav et al., 2021).

The complex water–rock interactions and geochemical processes governing the hydrogeochemical evolution of various aquifers, as well as the appropriateness of groundwater quality over Uttar Pradesh, were attempted by many researchers in the recent past (Raju et al., 2009; Singh et al., 2011; Raju et al., 2012; Chabukdhara et al. 2017; Mishra et al., 2018; Tyagi and Sarma 2020; Madhav et al., 2021). Raju et al., (2009) studied the groundwater quality of the Lower Varuna River basin. It proficiently revealed the water–rock interactions, controlling hydrogeochemical evolution and nitrate and fluoride contamination in quality assessment. Moreover, a similar study was conducted in the Varanasi urban area (Raju et al., 2012; Singh et al., 2015; Mishra et al., 2018), which again reported elevated nitrate concentration. Additionally, the study of trans-Varuna River basin hydrogeochemistry and its health implications conducted by Madhav et al. (2021) signified the rock dominance
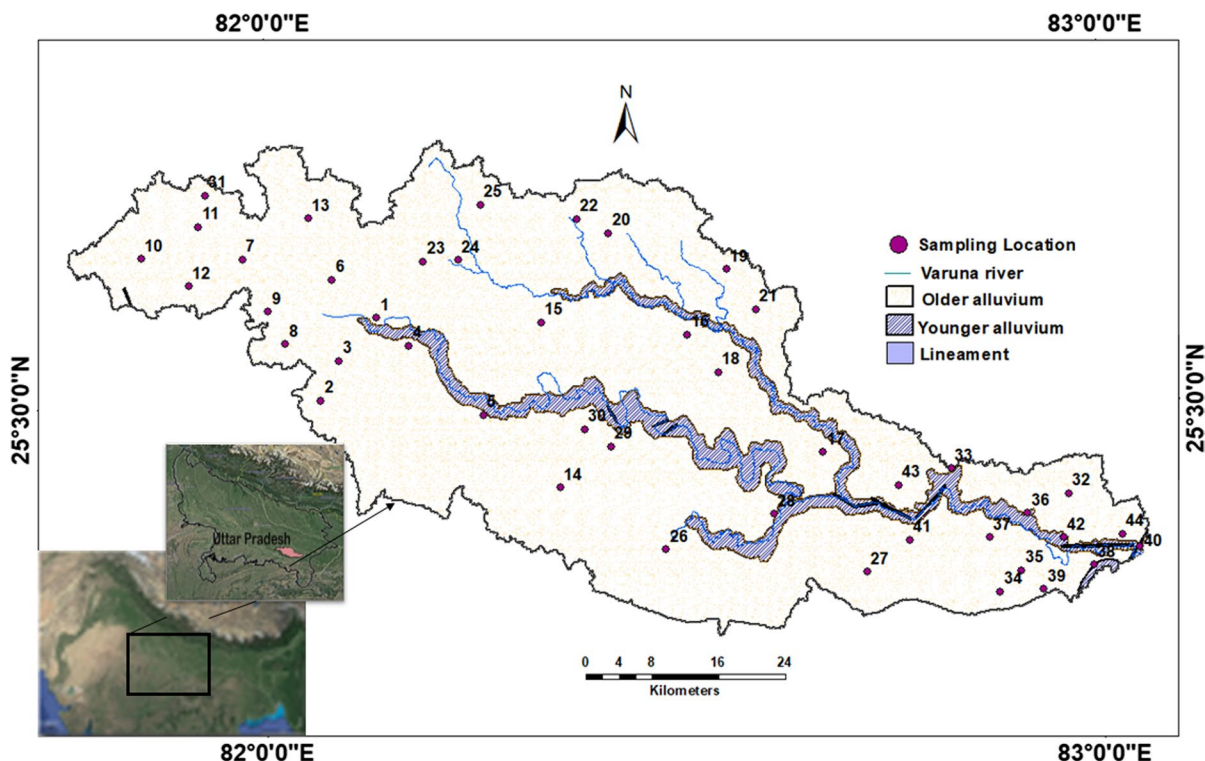
Fig. 1 Location and geology of the study area

origin, supersaturation of silicate and iron minerals, and vulnerability of nitrate contamination to infants and children. Hence, the existing studies generally focused on parts of the Varuna River basin. A comprehensive geochemical modeling and qualitative assessment associated with human health risk in the entire river basin has been unexplored, and thus, very little literature is available on the same aspect. Therefore, in view of the above fact and to fill the gap, the current study focuses on firstly presenting the hydrogeochemical status and formation mechanisms of groundwater resources in alluvial aquifers through an integrated application of stoichiometric analysis, thermodynamic stability analysis, and inverse geochemical modeling approach using PHREEQC, secondly, to understand the qualitative status using entropy water quality index (EWQI) for consumption and thirdly, to evaluate expected risks on human health implications based on the excessive occurrence of chemical constituents. Overall, the study puts effort into providing new insights for locally and socially appropriate attributions and optimization to manage groundwater infrastructure at a specific site.

Materials and methods

Study area and hydrological framework

The Varuna River basin (Fig. 1) is situated in Ganga's central alluvial plain and is an active agricultural region. The catchment area covers 3675 km^2 and has a stretch over the district of Varanasi, Allahabad, Sant Ravidas Nagar, and Jaunpur districts. This semi-arid to sub-humid area lies between 25°39′28″ N and 25°19′44″ N latitude and 81°45′57″ E and 82°03′06″ E longitude. The southwest monsoon brings the rainy season, with annual precipitation ranging from 572 to 897 mm. The temperature difference between summer and winter is considerable. The maximum temperature ranges from 22 to 48 °C, while the minimum temperature ranges from 15 to 1 °C.

The geological structure of the study area represents a stratigraphic profile of the Middle Pleistocene to the Holocene ages. The site is situated mainly over the Gangetic foreland, the redeposited sediments of the Siwalik thrust sheets (Singh, 1996). The Quaternary Alluvium formations rest in the basement

consisting of the Vindhyan group of rocks of the Pro- terozoic system. Deposition of medium to coarse sand and clay with kankar of the older alluvium of Middle Pleistocene to Upper Pleistocene predominates the area. The younger alluvium of the Upper Pleisto- cene-Recent associated with the river courses of the Varuna mainly consists of fine-grained sand, silt, and clay. Sand deposition and a low-energy fluvial phase due to the clay deposition over the river basin reflect intense fluvial activity (Singh et al., 2016). According to the subsurface succession, the shallow aquifer has clay, silt, and silty clay horizons, primarily compris- ing the unconfined aquifer. The primary components of the Older (Bhangar) and Younger (Khadar) allu- vium are Himalayan-acquired greywacke sediments with local beds of craton-acquired arkosic sand. These cover the upper layer and are visible on the sur- face in cliff parts along river banks (Dey et al., 2021a; Shukla et al., 2012).

The study area comprises over-exploited (23%) and semi-critical (31%) groundwater resources owing to unrestrained groundwater usage (CGWB, 2021; Dey et al., 2021a). The probable reason may be that a substantial rise (16%) in the populace from 2001 to 2011 increases the quest for groundwater to meet drinking/domestic water usage and agricultural needs (Dey et al., 2021b; Mall et al., 2006). It is one of India's most agriculturally productive regions owing to rich alluvium soil. The monsoon season provides sufficient water to the water table, but the pre-mon- soon season usually affords insufficient groundwa- ter withdrawal. The water table in this area occurred within confined and unconfined conditions. The shal- lower aquifers present down to the depth of 50–60 mbgl. Generally, most of the area's open and shallow tube wells become almost dry in the pre-monsoon season due to clay substances. The deep tube wells ranged from 250 to 400 m below the ground level. The alluvial fills are about 200–600 m thick and mul- tifaceted, with tiny clay layers at the top and the sub- surface regions (Dey et al., 2021a). The thick sand layers provide sufficient porosity and permeability to form a profuse aquifer; hence, the deep aquifers are more productive.

Data acquisition and quantification strategy

The collection of 88 representative groundwater sam- ples (Fig. 1) was integrated over two different seasons (44 each in pre-monsoon, May 2017 and post-mon- soon, October 2017) for the seasonal variations of hydrogeochemical parameters (Ca, Mg, K, Na, HCO_3, Cl, SO_4, NO_3, and F). The study used precleaned 1-L capacity polyethylene containers for water sam- ple collection. The sampling procedure involved the water collection after pumping for 10 min in the case of a bore well and filtered by Whatman filter paper before analysis. Major ions (Na, K, Ca, and Mg among major cations and HCO_3, Cl, SO_4, NO_3, and F among major anions) were examined using an ion chromatograph (Metrohm; 930 Compact IC, Switzer- land; Metrosep C4 (for cation) and MetrosepA Supp. 5 (for anion)). A portable Hanna combo meter meas- ured TDS (Total Dissolved Solids), EC (Electrical Conductivity), and pH at the time of sampling. Total hardness (TH) was estimated by the titration method. The IBE (ionic balance error) (Eq. 1) was computed to approve the correctness of the analysis, which was determined to be within the acceptable range of 1–10% (Domenico & Schwartz, 1990).

$$IBE = \frac{(O - R)}{(O + R)} * 100 \tag{1}$$

where IBE is in percentage, O and R are the meas- ures of the total cations and the total anions in meq/L, respectively. Instrumental and manual caused reagent slipups, limitations of methodologies, presence of contaminants in distilled water, and other factors all contribute to errors in groundwater chemical analysis.

The elementary chemical characteristics and spa- tial variability of groundwater were summarized using descriptive statistics. Additionally, the inter- relationship between the responsible parameters was investigated by correlation analysis. Further, the Piper diagrams (Piper, 1944) using AquaChem 4.2 soft- ware and different ratios of primary ions were used to determine the hydrogeochemical properties of groundwater.

Geochemical modeling approach

Inverse modeling works under a few conventional assumptions (1) the starting and final water wells selected for analysis should signify the same ground- water flow path, (2) groundwater chemistry is unaf- fected by dispersion and diffusion, (3) during the time considered, the aquifer system is in a chemical

steady-state, and (4) the aquifer should contain the phases (minerals) utilized in the reverse calculation (Chung et al., 2020). Inverse modeling in PHREEQC can predict the steady evolution of hydrochemistry in a given area along a groundwater flow path using saturation indices (Parkhurst & Appelo, 2013). A water table contour map was used in the present study to select starting (initial) and final positions by considering the general groundwater progression. Possible phase mole transfers were then calculated in the groundwater system by considering the starting and ending water composition differences (Roy et al., 2020). Accordingly, the program began by introducing the key phases (gases and minerals) along the flow path. The model initially ran across a predefined flow line. Potential phases were inhibited (precipitation/dissolution) by considering the overall trend in chemical concentrations and saturation indices. Oversaturated phases were permitted to precipitate, and undersaturated phases were allowed to dissolve (Parkhurst & Appelo, 2013). The model simulations were quantified with specific uncertainty limits (0.025 or 0.05 as default). The models ran onward using the ''minimal'' identifier. Accordingly, the uncertainty for the individual inverse model from the PHREEQC program was calculated considering the residual sums and maximum elemental fractional error (Sharif et al., 2008).

Drinking/domestic quality assessment

Conventional EWQI (Entropy Water Quality Index) had been occupied to assess drinking water quality based on hydrogeochemical parameters. Entropy-weighted methods represent an advanced form of water quality index, reduce the biases by comprehensive probabilistic weighting method, and upsurge the acceptability in several fields of hydrogeology and water quality (Amiri et al., 2014; Maskooni et al., 2020; Xiao et al., 2021). Shannon introduced entropy as a measure of uncertainty (Shannon, 1948) for the first time. Again the degree of biasness is inversely proportional to the prediction of a probabilistic occurrence (Maskooni et al., 2020). Hence, the method may mathematically capture the randomness of aquifer water quality accounting for the responsible parametric changes. A significant shift in parameter concentration will lead to a more considerable/ minor Shannon weight (Maskooni et al., 2020). In this study, the BIS (Bureau of Indian Standards) and the WHO (World Health Organization) guidelines (BIS, 2012; WHO, 2017) were used to compute the quality rate of the hydrogeochemical parameters (Table 1). Systematic calculations of this index are presented in supplementary section A. To evaluate groundwater quality based on the EWQI value, categories into excellent (<25), good (25–50), medium (50–100), poor (100–150), and extremely poor (>150).

Risk assessment of human health

Appraisal of health risk assessment estimates the degree of hazard in the presence of toxic elements in groundwater consumed for a certain period. According to the USEPA health hazard assessment model (USEPA, 2022), potential human health risks due to drinking and domestic use are the function of age, gender, body weight, time, and frequency of water consumption (Adimalla et al., 2020; Xiao et al., 2021). The risk level can be quantified as a noncarcinogenic health hazard caused by nitrate and fluoride consumption through ingestion absorption pathways from groundwater. Nitrate and fluoride are two important pollutants that harm human health in the noncarcinogenic aspect. In the present study, the population was categorized into two age groups, adult males and females (>18 years) and children (<18 years), and was proceeded for integrated health hazard index (HHI) evaluation. Detailed computation methods are described in the supplementary section (B).

Result and discussion

Physicochemical attributes

The concentration of the pH in the study area fluctuates from 6.89 to 8.65 (mean value of 7.65) in the pre-monsoon and 6.9 to 8.03 (mean of 7.61) in the post-monsoon, indicating an alkaline environment (Table 1) which suggests the incursion of carbonates into the aquifer functioning between soil and rainwater (Kumar et al., 2018). The pre-monsoon EC in the examined area varies from 510 to 3510 μS/cm. The post-monsoon EC ranges from 580 to 2260 μS/cm, indicating long-term hydrogeochemical processes favor the salinity intensification. The concentration of TDS (total dissolved

Table 1 Descriptive statistics of ground water samples of the study

Parameters	PH		EC		TDS		TH		Na$^+$		K$^+$		Mg^{2+}		Ca^{2+}		HCO$_3^-$		Cl$^-$		SO$_4^{2-}$		F$^-$		NO$_3^-$	
	Pre	Post	Pre	Post	Pre	Post	Pre	Post	Pre	Post	Pre	Post	Pre	Post	Pre	Post	Pre	Post	Pre	Post	Pre	Post	Pre	Post	Pre	Post
Max	8.65	8.03	3510	2260	1760	1130	552.7	598.1	224.1	289.4	12.7	14.5	76.8	87.1	95.1	96.3	664.0	724	224.1	227.8	183.4	220.8	2.3	2.7	57.5	58.8
Min	6.89	6.9	510	580	250	290	116.3	278.4	1.5	32.5	1.7	1.55	10.5	11	11.1	21.5	185.0	222	1.5	12.4	2.6	13.6	0.5	0.34	0.3	0.6
Mean	7.69	7.61	943.2	1001.8	471.1	500.9	219.4	278.4	68.2	87.7	4.9	5.6	31.9	38.4	35.4	48.4	316.0	374.8	42.5	55.0	27.3	39.3	1.0	1.07	19.2	22.6
SD	0.49	0.23	524.9	1001.7	262.2	218.6	71.9	82.9	29.3	39.5	2.4	2.8	12.5	14.1	15.1	16.7	106.9	109.7	44.0	39.8	27.4	30.6	0.4	0.53	16.5	16.1
No. of samples Exceeded limit	3	2	4	6	9	23	28	39	1	1	–	–	25	33	1	5	–	–	/	/	/	/	6	8	6	5
Standards as per[a]WHO/[b]BIS guidelines	6.5–8.5[a]		1500[a]		500[a]		200[a]		200[a,b]		–		30[a]		75[a,b]		–		250[a,b]		200[a,b]		1.5[b]		45[a]	

---

solids) in the groundwater samples varies from 250 to 1760 mg/L (mean 471 mg/L) in pre-monsoon and 290 to 1130 mg/L (mean 500 mg/L) in post-monsoon (Table 1). According to TDS values (Freeze & Cherry, 1979), 95% and 5% of pre-monsoon groundwater samples and 93% and 7% of groundwater samples of post-monsoon are classified as fresh and brackish, respectively. According to the USGS-TH classification (Sawyer & Mc Carty, 1967), 81% of pre-monsoon and 73% of post-monsoon samples are classified as hard, and groundwater samples of 9% (each in pre-monsoon) and 25% and 2% (in post-monsoon) are classified as mild hard and very hard in nature (Table 2).

Relative cations concentration in the study region shows the order of Na > Ca > Mg > K, and the dominant anions order is HCO$_3$ > Cl > SO$_4$ > NO$_3$ > F (Supplementary Fig. 1). The predominance of sodium may be due to salt dissolution regulated by evaporation (Subba Rao et al., 2020). At the same time, the potassium concentration (70%) is less than 5 mg/L, indicating that the country rock has a higher solubility behavior due to potassium ion retention in clay minerals (Hem, 1991). Moreover, the existence of kankar in the area, coupled with a sodium concentration twice that of calcium, shows Ca and Na exchange ions (Subba Rao et al., 2020). The abundance of Mg in pre-monsoon and post-monsoon are 23% and 21%, respectively, which is near the quantity of Ca (in pre-monsoon, 25% and post-monsoon, 26%). The presence of CO$_2$ in the soil zone administers both concentrations. Generally, in terms of solubility, Ca is more soluble than Mg in a natural condition (Hem, 1991). More abundance of Mg is also maybe the product of anthropogenic activity.

The most dominant anion, HCO$_3$, represents the major source of alkalinity. A significant variation was observed in the HCO$_3$ spatial distribution at specific locations. The preponderance of bicarbonate indicates the role of the carbonate weathering process, which involves H$_2$O and CO$_2$ generated through the respiration of roots and decomposition of organic matter in the soil zone to generate HCO$_3$ (Raju et al., 2011; Subba Rao et al., 2020). Cl is primarily obtained from non-lithological sources (Hem, 1991), such as poor hygienic conditions and irrigation practice impacts. SO$_4$ is a gypsum product used to reform soils' physical/chemical qualities to improve drainage and irrigation (Todd, 1980). In the study region, six samples

Table 2 Groundwater classifications and quality assessment on the basis of physical parameters and EWQI

	Water class	Premonsoon		Postmonsoon	
		No of samples	% Samples	No of samples	% Samples
USGS Total Hardness(mg/L)					
0–75	Soft	–	–	–	–
75–150	Mild Hard	4	9.1	1	2.3
150–300	Hard	36	81.8	32	72.7
>300	Very Hard	4	9.1	11	25
TDS (mg/L) (Davis and Dewiest 1967)					
<500	Desirable for drinking	36	81.8	31	70.5
500–1000	Permissible for drinking	6	13.6	10	22.7
1000–3000	Useful for irrigation	2	4.5	3	6.8
>3000	Unfit for drinking and irrigation	–	–	–	–
EWQI					
<25	Excellent	20	45	22	50
25–50	Good	17	39	10	23
50–100	Medium	5	11	10	23
100–150	Poor	2	5	2	5
>150	Extremely poor	–	–	–	–

	Water class	Premonsoon		Postmonsoon	
		No of samples	% Samples	No of samples	% Samples
EC Richards (1954)					
<250	Excellent	–	–	–	–
250–750	Good	17	38.6	15	34.1
750–2250	Permissible	25	56.8	28	63.6
>2250	Doubtful	2	4.5	1	2.3
TDS (mg/L) (Freeze & Cherry, 1979)					
<1000	Fresh	42	95.5	41	93.2
1000–10,000	Brackish	2	4.5	3	6.8
10,000–100,000	Saline	–	–	–	–
>100,000	Brine	–	–	–	–

of pre-monsoon and five samples of post-monsoon surpassed the desired level of nitrate. Nitrate infiltration enhances coarse and highly porous alluvial soil but is restricted by compact clayey soils (Raju et al., 2009). However, excess concentration of NO_3 reflects the anthropogenic sources. The active dissolving of F-bearing minerals in country rocks favored by an alkaline environment may influence F concentration in groundwater. Other than that, the anthropogenic approach may contribute to fluoride in groundwater. Fluoride concentration varies between 0.5 and 2.3 mg/L in pre-monsoon and 0.3 and 2.8 mg/L in post-monsoon. The permissible limit was exceeded by six and eight samples, respectively, in pre-monsoon and post-monsoon. The concentration specifies susceptibility for dental fluorosis than skeletal fluorosis.

Hydrogeochemical facies

Hydrogeochemical facies accredit the extent of rock–water interaction and focus on the residence time, geology, and regional flow pattern of subsurface water (Kumar et al., 2018). The traditional trilinear diagram by Piper (1944) characterizes the hydrogeochemical facies. According to the triangular fields of the diagram (Fig. 2), 86% of groundwater samples fall into the no dominance type, while 9% fall into sodium and 5% fall into magnesium types in the

cation facies for both seasons. Except for two samples (48, 49) from the post-monsoon season, all groundwater samples in the anion facies fall into the bicarbonate type. The diamond field (Fig. 2) captures the combined effect of cations and anions on water type. The plot reveals that most of the groundwater samples (93% in pre-monsoon and 89% in post-monsoon) remained in the sub-fields 1, 3, and 5, signifying alkaline earth exceeds alkalis, weak acids outdo strong acids, and the presence of carbonate hardness (secondary alkalinity), respectively. The remaining samples are in field 9, demonstrating that no cation–anion pair exceeds 50% in mixed water. Hence, the dissolution of minerals, ion exchange, and freshwater recharging may provide Ca–Mg–HCO3 water type. Moreover, for both seasons, alkaline earth and weak acids dominate the entire hydrochemistry, characterized by temporary hardness (or carbonate hardness). The overall geochemical classification suggests the geochemical processes during infiltration of recharge water as the source of soluble solids in the groundwater of the study area.

Characterization of hydrogeochemical processes

Explicit determination of stoichiometric relations (e.g., mole ratio) marked the internal mechanism responsible for obtaining hydrochemistry and specific sources (Hem, 1991). Water–rock interaction

Fig. 2 Piper trilinear diagram showing the hydrogeochemical facies of groundwater samples (*after* Piper, 1944)
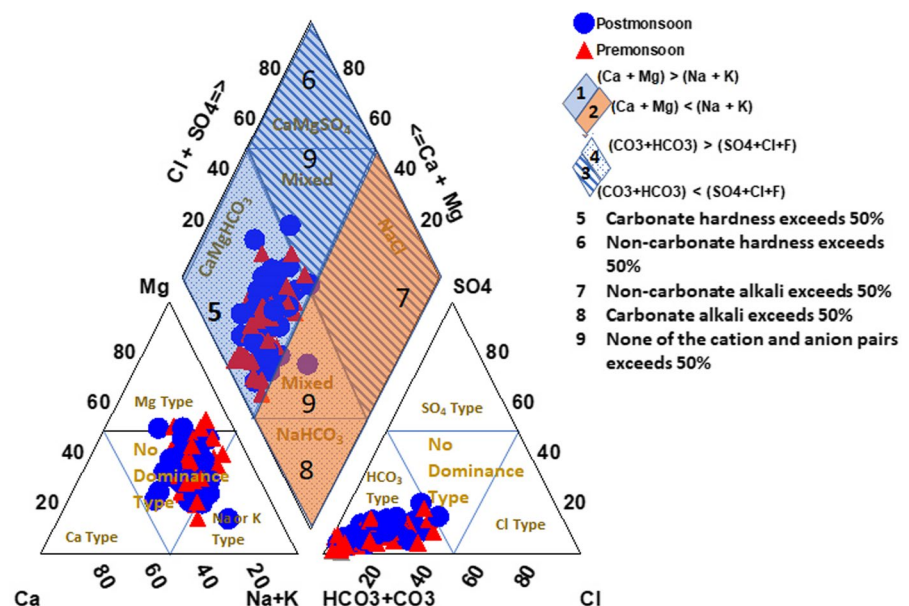
is the function of three foremost procedures, i.e., weathering of silicate, carbonate, and evaporite. The logarithmic bi-dimensional plots of the Na—normalized molar ratios HCO$_3$/Na vs. Ca/Na, and Mg/Na vs. Ca/Na can represent specific weathering in the aquifer environment (Fig. 3). Samples with a lower Na- normalized ratio are that of the product of silicate weathering. The Ca/Na ratio of in situ rocks is approximately 0.6 for both seasons. In the silicate weathering process, highly soluble Na increases the Na concentration in aqueous media; hence, a lower ratio is expected for the Ca/Na ratio (Patel et al., 2016). The average value of the Ca/Na ratio is near the reference value, signifying the silicate weathering dominancy (Table 3). The existence of silicate-based geology in the area satisfies the fact. However, the regression between Ca/Na and HCO$_3$/Na ($R^2 = 0.338$ in pre-monsoon and 0.3427 in post-monsoon) and Ca/Na and Mg/Na ($R^2 = 0.1782$ in pre-monsoon and 0.041 in post-monsoon) reveals low to moderate positive regression, implying that silicate weathering has a limited impact on the hydrogeochemical components in the study region. Generally, high Na-normalized ratios can be achieved due to weathering conditions where Ca-rich minerals are especially dissolved, showing an almost symmetrical dispersal for Ca/Na ratios (Fig. 3). However, post-monsoon data showed slightly positive skewness, indicating the presence of weathering of carbonate and ion exchange processes (Gaillardet et al., 1999).

In addition, Na transfers due to weathering of silicate from feldspars or human-induced activities (Patel et al., 2016) are typically interpreted by the variation in the Na/Cl molar ratio of more than one. Except for samples no. 1, 2 (pre-monsoon) and samples no. 4, 32 (post-monsoon), all of the samples in this study had a molar ratio more than or equivalent to 1, representing that ion exchange is the primary procedure that is exchanged by silicate weathering rather than halite dissolution. The Na vs. Cl scatter plot (Fig. 4) also demonstrates most of the samples lie above the 1:1equiline, suggesting no halite
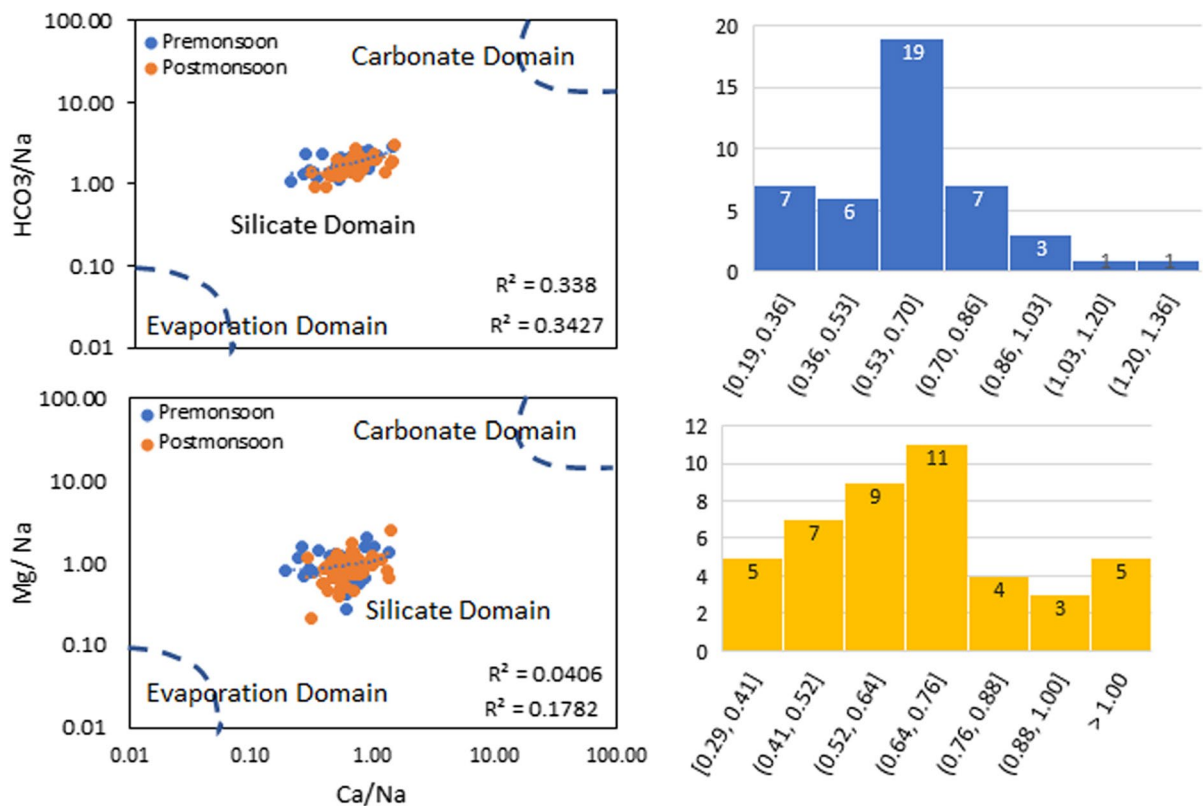

Fig. 3 The plot of Na-normalized molar ratios to determine the prevailed weathering environment.

Table 3 Stoichiometric relations (molar ratio) marked the internal mechanism responsible hydrochemistry

Indices	Seasons (meq/l)		Internal responsible mechanism for hydrochemistry
	Pre	Post	
Ca^{2+}/Na^+	0.62	0.69	The presence of coupled weathering of silicate and Carbonate minerals
Mg^{2+}/Na^+	0.95	0.91	
HCO_3^-/Na^+	1.82	1.71	
$Ca^{2+}+Mg^{2+}/TZ^+$	0.57	0.58	
$Ca^{2+}+Mg^{2+}/HCO_3^-$	0.87	0.93	Cation Exchange of Ca and Mg by Na in silicate minerals
Ca/HCO_3^-	0.34	0.4	
Ca^{2+}/Mg^{2+}	0.75	0.84	Dissolution of dolomite
Na^+/Cl^-	5.3	3.21	Ion exchange in silicate minerals and confirms no halite dissolution
CAI-1	− 4.7	− 2.43	Reverse ion exchange
CAI-2	− 0.33	− 0.33	
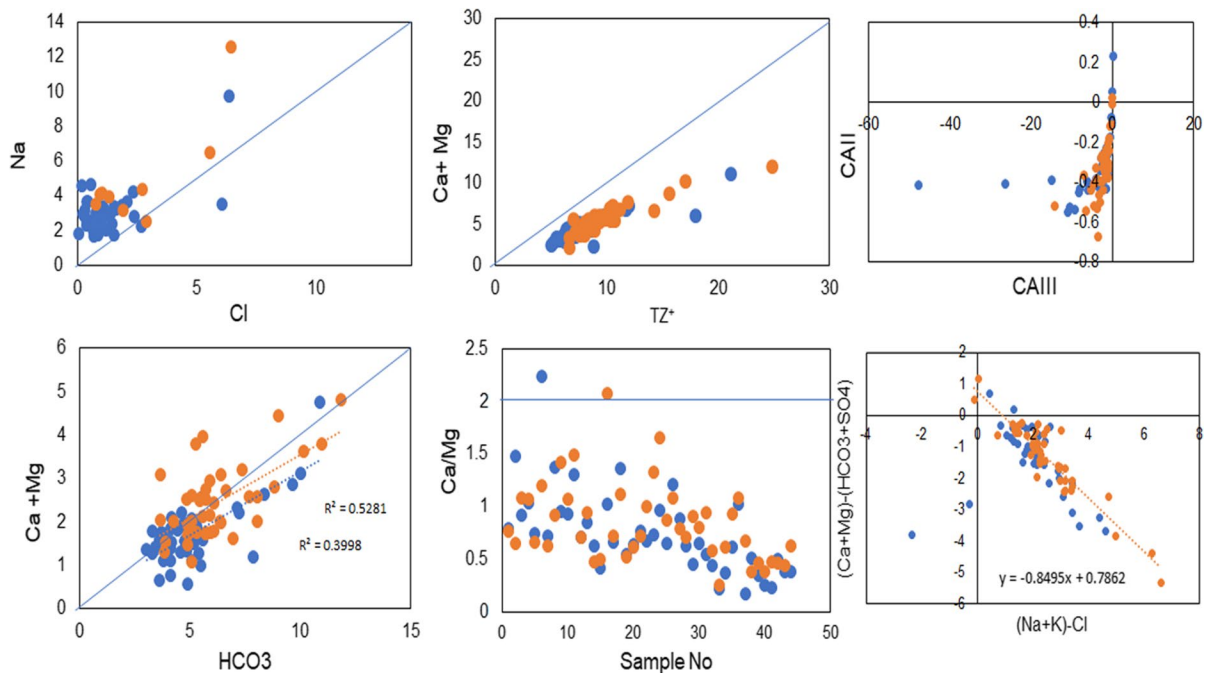
Fig. 4 Scatter plot showing stoichiometric relations between ions.

dissolution. Hence, Na may be derived from silicate dissolution in the study region since the groundwater that originates solvents chiefly by weathering of silicate would show HCO_3 dominancy (Fisher & Mullican, 1997). HCO_3 may be a consequence of weathering of feldspar minerals derived from aquifer composition with the presence of carbonic acid in the groundwater (Patel et al., 2016) (Supplementary Section C). The correlation analysis strongly supports the combined sources (Fig. 5). Ca, Mg, Na and HCO_3 have a strong correlation with each other, suggesting rock weathering sources. In contrast, Na strongly correlates with Cl which specifies the anthropogenic sources. Furthermore, TDS shows a strong correlation with all other parameters except K, F, and NO_3 (Fig. 5). Hence, it rejects the geogenic origin of both F and NO_3. K is generally found in low concentration due to the high
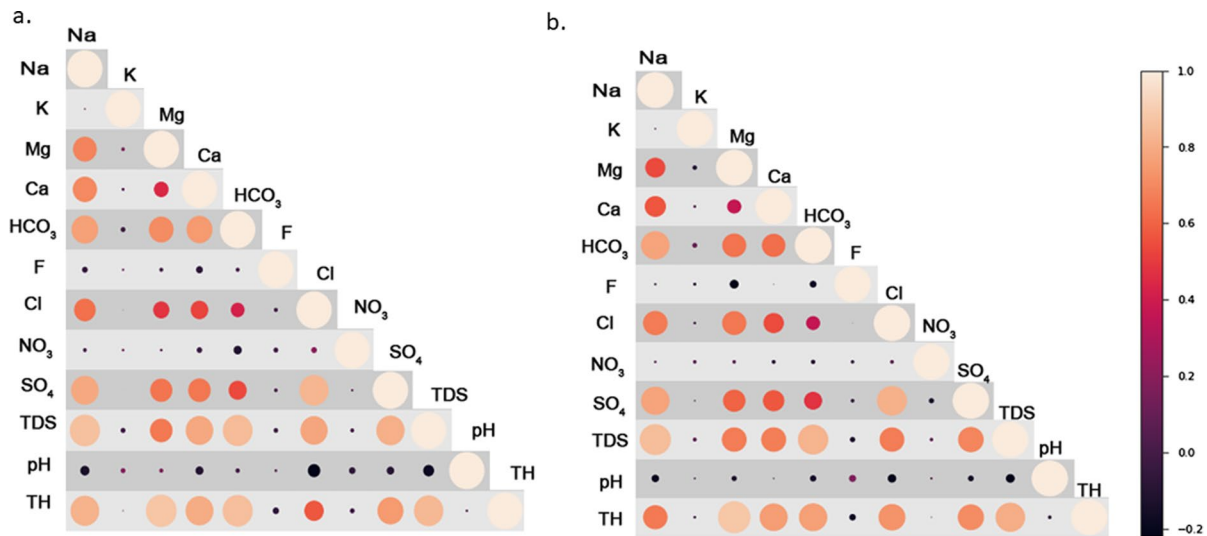
Fig. 5 Pearson correlation between the physico-chemical parameters of the groundwater samples **a** Premonsoon **b** Postmonsoon

resistance to weathering, which shows an almost negative correlation with others.

The molar ratio and plot (Fig. 4) of Ca+Mg vs. TZ^+ (total cations) show that the chemical data lie below the theoretical line (1:1) and are close to the 1:0.6 line (Ca+Mg=0.6TZ^+), indicating that degradation of silicate arises in addition to the dissolution of carbonate (Raju et al., 2016). Significantly, the evidence for weathering of silicates may also be elucidated in the plot HCO_3 versus Ca+Mg. Calcium and magnesium are introduced to the groundwater at a slower pace relative to HCO_3 as most of the samples lie below equiline, and the data cluster around 1:1. In addition, the lower Ca/HCO_3 molar ratio (<0.5) is observed in the groundwaters of the study area (Table 3), probably due to either HCO_3 augmentation from silicate weathering or the cation exchange involving magnesium and calcium in water by sodium fixed in clay (Liu et al., 2021). Gypsum and carbonate weathering seem to be primarily responsible for the observed quantity of Ca+Mg in groundwater in the studied area. Limestone, dolomitic limestone, dolomite, and kankar are significant carbonate sources (Raju et al., 2016). The dolomite and calcite dissolution in the alluvium of the study region may be judged by the Ca/Mg molar ratio of the groundwater. The molar ratio Ca/Mg=1 represents the dissolution of dolomite, whereas a higher ratio indicates a more significant contribution of calcite. The dissolution of

silicate minerals, which promotes calcium and magnesium in groundwater, is characterized by a high Ca/Mg ratio (>2) (Patel et al., 2016). The lower average molar ratio of Ca/Mg (0.75 and 0.83 in pre-monsoon and post-monsoon season, respectively) specifies the dolomite dissolution (Table 3). Only one sample (sample no. 6 in the pre-monsoon and sample no. 16 in the post-monsoon) is above the molar ratio line 2, showing the influence of silicate minerals (Fig. 4). Ca+Mg/ HCO_3 has a mean ratio of 0.87 in pre-monsoon and 0.93 in post-monsoon (Table 3), suggesting that Ca and Mg are not exclusively derived through carbonate dissolution and may be attributed chiefly to gypsum and carbonate weathering (Sami, 1992).

Groundwater chemical composition is acquired from the aquifer material owing to the ion exchange at traveling and residency and can be comprehended by the chloro-alkaline indices (CAI) (Supplementary Section C). Both indices should be positive when ion exchange occurred between the aquatic Na and adsorbed Ca in sediment. However, in the deposition, aquatic Ca substitutes adsorbed Na, and both indices are negative (Liu et al., 2021). CAI I and CAI II are both negative in most of the cases (except samples 1 and 2 in pre-monsoon and sample no. 32 in post-monsoon), representing that reverse ion exchange is dominant in the study region (Fig. 4).

The cation exchange process is ambiguously determined by the plot of (Na+K–Cl) vs.

(Ca + Mg)–(HCO$_3$ + SO$_4$) (Fig. 4). Specifically, calcium and magnesium are balanced by HCO$_3$ and SO$_4$. In contrast, Na and K are balanced by Cl, mainly derived from carbonate and silicate weathering and salt dissolution in a subsurface environment. The significant effect of the process would lead the plot to a negative slope ($y = -x$) (Patel et al., 2016). The maximum observed data show a negative slope ($y = -0.96$ in pre-monsoon and -0.85 in post-monsoon) except for two samples (ID 1 and ID 2). These two samples show positive CAI indices and have high chloride concentrations, indicating anthropogenic contribution through ion exchange processes. Almost all the data points lie in the second quadrant, implying that (HCO$_3$ + SO$_4$) is dominant over Cl in the subsurface waters. Excess concentration of Na in groundwaters also clearly explains the exchange of cation between calcium or magnesium and sodium (Jalali, 2010). Exchange processes between Ca-Na within the clay environment resulting in diminution of Ca and Mg relative to the increment of Na may also be noticed through the Na/Cl ratio higher than 1 (Table 3) (Patel et al., 2016).

Geochemical modeling

Water–rock interactions and electron transfers are generally slow chemical reactions (Wernberg, 1998). Time is a factor in elementary kinetic reactions, as seen in the case of quartz solution, which requires thousands of years to reach complete equilibrium (Rimstidt, 1997). Hence, water–rock stability essentially includes the evolutionary development of groundwater and enables incomprehensibly determining the relation between the degree of water saturation to minerals (Timoshenkova et al., 2014). Subtropical to tropical climates with high rainfall and well-drained settings are more likely to favor the weathering of primary silicate minerals to kaolinite, which can establish the chemical equilibrium in groundwater (Edet & Okereke, 2005). The study area shows a steady kaolinite phase during both seasons (Supplementary Fig. 2) that refers to a well-established groundwater drainage system that allows anorthite and albite to disintegrate insufficiently to generate kaolinite and other secondary products. (Appelo & Postma, 2005).

In contrast, the study region is undersaturated with albite, and anorthite would allow the further dissolution of these minerals (Fig. 6). In the lower crust of sedimentary basins, one of the most frequent alumino-silicate reactions is albitization. It also reflects mass transfer and causes chemical changes in subsurface pore fluids (Perez et al., 2005). The groundwater stability in the kaolinite stability fields is also demonstrated by the K–Al silicate and Mg–Al silicate phase diagrams, which show incompatible weathering of muscovite and k-feldspar, respectively. Saturation indices of the study area show supersaturation with the minerals mentioned earlier and illite, which is usually an alteration product of muscovite. Generally, illite can be regarded as the weathering product of a process where muscovite maybe eventually altered to montmorillonite. Montmorillonite formation may result from the solid interplay of groundwater–silicate minerals (longer residence time) with the restricted groundwater flow in semi-arid conditions (Raju, 2017). Eventually, the mineral saturation indices indicate the dissolution and precipitation of the aluminosilicate minerals Ca-Montmorillonite, Gibbsite, K-feldspar, K-mica, Kaolinite, Illite, and a part of Chlorite (Fig. 6), which are relatively common in the local soils.

Partial CO$_2$ (g) pressures in the area range between -3.35 and -1.25 in pre-monsoon and -2.69 and -1.2 in post-monsoon, indicating greater pCO$_2$ relative to the atmospheric value (around -3.5) and biological activity in soils. Hence, carbonate minerals dissolve first in the aquifer, latterly, in silicates (Gueroui et al., 2015). The observed supersaturation of quartz and chalcedony suggests excess Si derives from amorphous Si. However, amorphous silica is undersaturated in groundwater, indicating that it is imbalanced and would emit Si into the groundwater. As a result, high amounts of dissolved Si may stimulate significant silicate mineral breakdown in groundwater. Again, the precipitation enhanced the amount of kaolinite produced by the reaction of gibbsite with dissolved silica at a high pH (Supplementary Section C). Furthermore, with longer residence spans, kaolinite can react with cations (Ca, Mg, K, and Na) and silica to form smectites (Na or Ca-montmorillonite) or illite (Supplementary Section C).

Conversely, a vast part of the study region exhibits calcite (61.4% in pre-monsoon and 86% in post-monsoon) and dolomite (70.5% in pre-monsoon and 93% in post-monsoon) supersaturation. Aragonite (50% in pre-monsoon and 75% in post-monsoon) shows
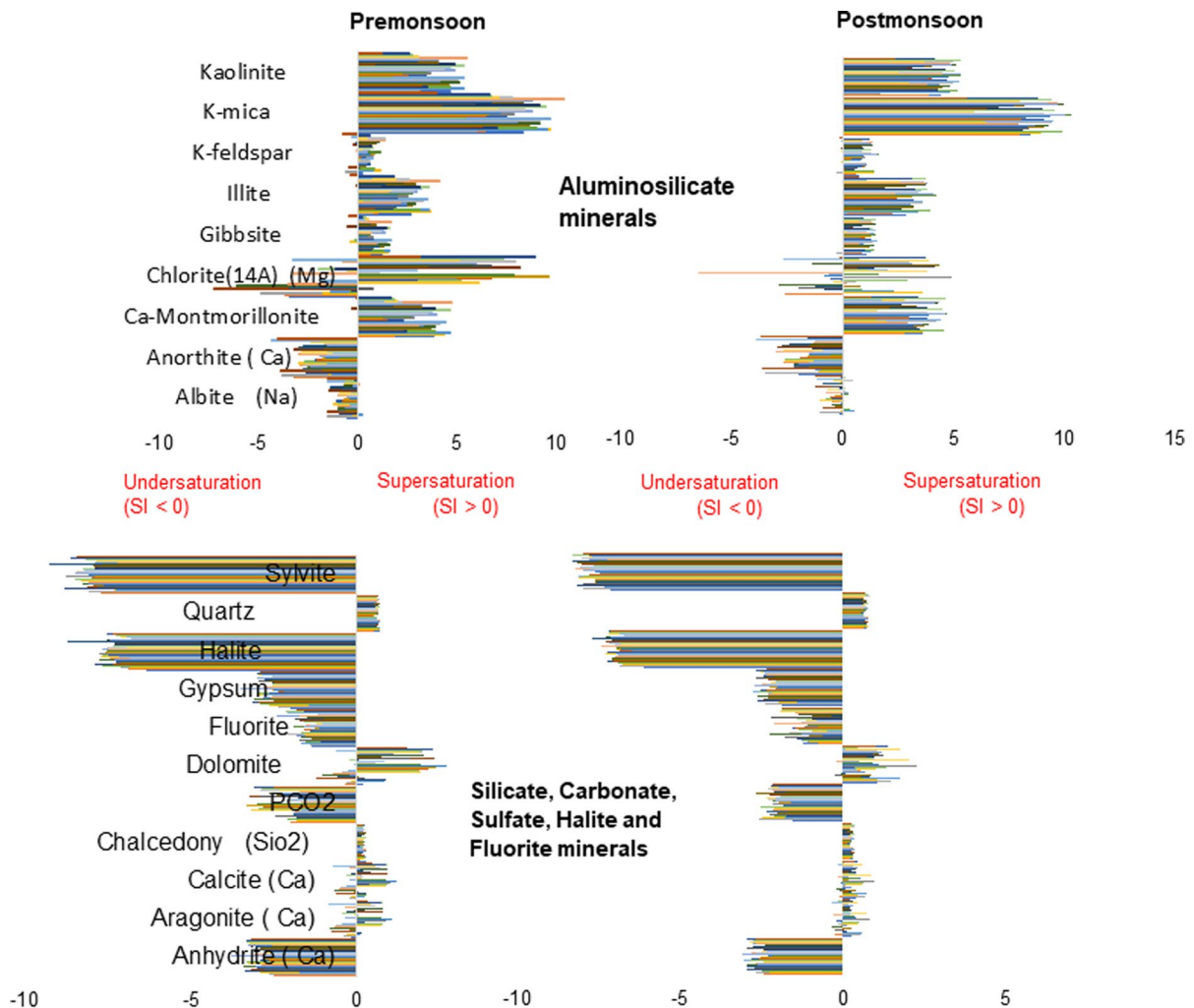
Fig. 6 Plot of saturation indices of different minerals

partial supersaturation in the system (Fig. 6). Unbalanced silicate weathering can induce the accumulation of Ca, Mg, and HCO_3 in groundwaters, which can aid in mineral disintegration.

A conceptual flow path was assigned by considering the area's elevation, water table distribution, and rainfall distribution (Fig. 7). The study area was eventually divided into three sections. Inverse models were then created to study hydrogeochemical changes within the three basic categories. The mean physiochemical input parameter of the groups was used to distinguish between starting (initial) and ultimate (final) groundwaters along a flow direction (Table 4). Group I is a highly elevated northeastern region, considered a recharge area with a

limited recharge as the region receives low rainfall with salt-affected areas (Fig. 7). Hence, the water received Na–HCO_3–Cl type, further transported to the central part of the area (Group II), received maximum rainfall and mineral dissolution, resulting in Na–Ca–HCO_3 water type. Group III represents a relatively low elevated southeastern part with low rainfall and a high water table. The geochemical concentration of Group III (Na–Mg–HCO_3) suggests the presence of carbonate dissolution along with silicate weathering. However, the Group characterized by low EC concentration offers reduced weathering activity, which may be primarily constrained due to the high settlement area (Fig. 7). The central part (Group II) represents the transitional zone and supports the
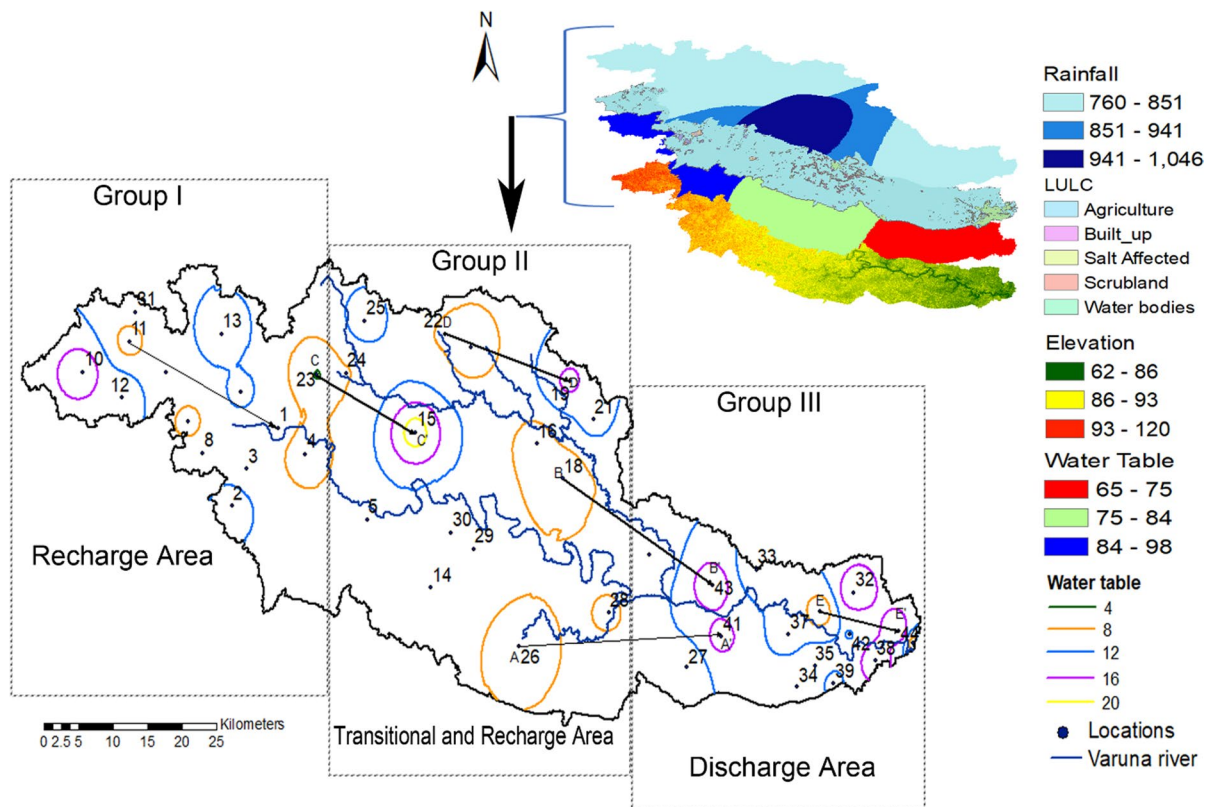
Fig. 7 Three groups of the study area depending on the parameters shown in thematic maps for inverse modelling
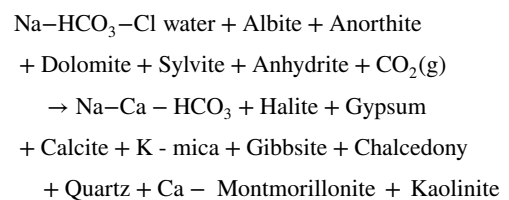
mixing processes. Consequently, Group I and Group III mixing simulations were studied. Using batch reaction in PHREEQC, mixing proportions of the two solutions ranged from 10 to 90% of both samples; the mixing calculation outcomes are shown in Table 5. It was found that 50% of each solution in pre-monsoon and 25% of Group I, and 75% of solutions of Group III in post-monsoon almost matched the composition of Group II. The model confirmed the mixing process. In the post-monsoon season, the proportion of Group III is higher than in the pre-monsoon season, which indicates more dissolution in post-monsoon and can also be due to the mobilization of the water in monsoon. Seasonal water table changes, groundwater withdrawal, transport processes caused by density gradient, diffusion and dispersion, geological formation features, and many other factors can all contribute to the mixing phenomena that emerge at aquifer interfaces. The disequilibrium among aquifer material

and groundwater promotes secondary mineral dissolution and precipitation, such as calcite, halite, gypsum, kaolinite, chalcedony, and others (Barzegar et al., 2018).

The primary processes of evolution of water chemistry, from Na–HCO$_3$–Cl type (Group I) to Na–Ca–HCO$_3$ type (Group II), can be structured by the following model using the results of inverse modeling (Table 6):
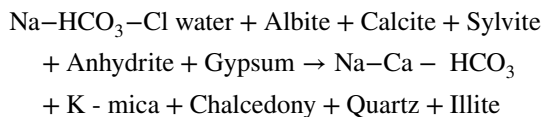
Model 1:

Pre-monsoon

$$\text{Na} - \text{HCO}_3 - \text{Cl water} + \text{Albite} + \text{Anorthite}$$
$$+ \text{Dolomite} + \text{Sylvite} + \text{Anhydrite} + \text{CO}_2(g)$$
$$\rightarrow \text{Na} - \text{Ca} - \text{HCO}_3 + \text{Halite} + \text{Gypsum}$$
$$+ \text{Calcite} + \text{K - mica} + \text{Gibbsite} + \text{Chalcedony}$$
$$+ \text{Quartz} + \text{Ca} - \text{Montmorillonite} + \text{Kaolinite}$$

Post-monsoon

Table 4 Mean parameter values of the three principal water groups

	Na		K		Mg		Ca		HCO$_3$		F		Cl		SO$_4$		SiO$_2$		TDS		EC		pH		Al	
	Pre	Post	Pre	Post	Pre	Post	Pre	Post	Pre	Post	Pre	Post	Pre	Post	Pre	Post	Pre	Post	Pre	Post	Pre	Post	Pre	Post	Pre	Post
Group I (Initial; n=13)	61.8	86.8	4.6	6.1	23.3	32.6	36.2	49.4	292.4	340.2	0.94	1.11	52.7	64.2	22.8	36.5	29.2	32.5	494.6	525.4	991.5	1053.1	7.3	7.6	0.03	0.03
Group II (n=17)	75.8	101.6	4.3	5.3	34.3	40.2	40.5	56.4	345.8	423.7	0.96	1.07	39.6	56.3	32.4	46.4	29.5	30.6	515.3	550.6	1028.8	1096.5	7.7	7.6	0.05	0.05
Group III (Final; n=14)	64.3	71.7	5.9	5.4	37.2	41.6	26.2	37.7	300.4	347.5	1.0	1.04	36.6	44.9	25.2	33.3	29.9	31.4	395.7	417.9	794.3	839.3	7.9	7.7	0.05	0.05

All values are in mg/l except pH and EC (μSiemens/cm)

$$Na-HCO_3-Cl\ water + Albite + Calcite + Sylvite + Anhydrite + Gypsum \rightarrow Na-Ca-\ HCO_3 + K\text{-}mica + Chalcedony + Quartz + Illite$$
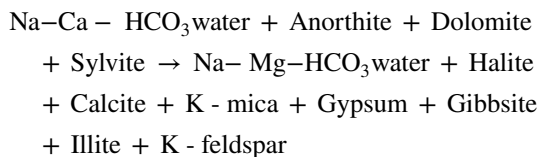
The model shows that in the pre-monsoon season, dissolved constituents in Group II waters are predominantly caused by weathering and dissolution of anorthite, albite, dolomite, anhydrite, and sylvite. Rainfall infiltration during the post-monsoon may dilute the groundwater and cause more calcite and gypsum dissolution. A relative increment in concentrations of Na, K, Ca, HCO$_3$, and Si suggests that silicate weathering and dissolution of carbonate are the primary factors for ion release. The evolution of the water chemistry along the flow path from Group II to Group III can be explained by the following equations.

Model 2:

Pre-monsoon

$$Na-Ca-\ HCO_3\,water + Albite + Anorthite + Dolomite + Sylvite + Anhydrite + Gypsum + CO_2(g) \rightarrow Na-Mg-HCO_3\,water + Halite + Calcite + Chalcedony + K\text{-}mica + Quartz + Ca-montmorillonite + Gibbsite + Illite$$

Post-monsoon

$$Na-Ca-\ HCO_3\,water + Anorthite + Dolomite + Sylvite \rightarrow Na-Mg-HCO_3\,water + Halite + Calcite + K\text{-}mica + Gypsum + Gibbsite + Illite + K\text{-}feldspar$$
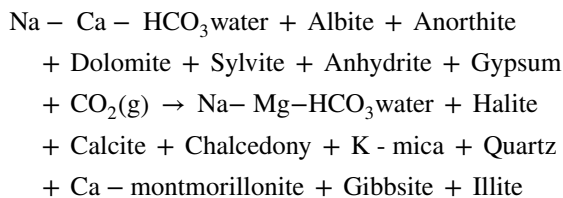
The modeling approach predicts albite, anorthite, dolomite, gypsum, anhydrite, sylvite dissolution, and precipitation of calcite, gibbsite, Ca-montmorillonite, kaolinite, K-mica, chalcedony, illite, quartz, and halite in the direction of flow. Weathering of silicate, dissolution of carbonate, and ion exchange processes are more dominant in pre-monsoon, which is justified by the precipitation of chalcedony and Ca-montmorillonite. The high magnesium concentration in Group III groundwaters is probably associated with the ionic exchange progressions. The critical phase transformations along the flow path are illustrated in Supplementary Table 2. The presence of halite for both seasons represents the saline nature of groundwater in the study area.

Table 5 Results of mixing calculations (in meq/l) of water groups using PHREEQC 3.6.2–15,100 (Minteq.V4 database)

Mixing elements	10% Group I+90% Group III		25% Group I+75% Group III		50% Group I+50% Group III		75% Group I+25% Group III		90% Group I+10% Group III	
	Pre	Post	Pre	Post	Pre	Post	Pre	Post	Pre	Post
HCO$_3$	5.95E-03	7.14E-03	5.84E-03	6.95E-03	5.65E-03	6.62E-03	5.84E-03	6.30E-03	5.34E-03	6.10E-03
Ca	6.79E-04	9.70E-04	7.16E-04	1.01E-03	7.78E-04	1.09E-03	7.16E-04	1.16E-03	8.78E-04	1.21E-03
Cl	1.08E-03	1.32E-03	1.15E-03	1.40E-03	1.26E-03	1.54E-03	1.15E-03	1.68E-03	1.44E-03	1.76E-03
F	5.24E-05	5.52E-05	5.19E-05	5.57E-05	5.11E-05	5.66E-05	5.19E-05	5.75E-05	4.98E-05	5.81E-05
K	1.47E-04	1.39E-04	1.42E-04	1.41E-04	1.34E-04	1.46E-04	1.42E-04	1.51E-04	1.20E-04	1.54E-04
Mg	1.47E-03	1.63E-03	1.39E-03	1.58E-03	1.24E-03	1.50E-03	1.39E-03	1.42E-03	1.02E-03	1.37E-03
Na	2.79E-03	3.19E-03	2.77E-03	3.29E-03	2.74E-03	3.45E-03	2.77E-03	3.61E-03	2.70E-03	3.71E-03
SO$_4$	2.60E-04	3.50E-04	2.57E-04	3.55E-04	2.50E-04	3.64E-04	2.57E-04	3.72E-04	2.40E-04	3.77E-04

Urbanization and agriculture are predominant land use in this part of the studied region. Uncontrolled urbanization brings up improper sewage collection into many wastewater pools that interact with freshwater aquifers and allow the accumulation of halite over time. Rising water levels and defrayal of vegetation cause salt accumulation in soils and groundwater. These salts are percolated down along with the precipitation. Besides that, repeated irrigation of water deposits salts in the land as residue after evaporation may concentrate over time. These concentrated salts soak the groundwater with precipitation, boosting the halite content.

Drinking/domestic quality assessment

Groundwater quality is greatly influenced by its hydrogeochemical parameter concentrations. Thus, it was compared to the standards set by BIS and WHO guidelines to measure the appropriateness for drinking, domestic, and public health uses (BIS, 2012; WHO, 2017) (Table 1). The study again considers the area's TDS and TH (Total Hardness) values and uses the EWQI (entropy water quality index) approach. Higher pH affects the mucous membrane and causes a bitter taste in groundwater. Except for three pre-monsoon samples and two post-monsoon samples, all samples are within acceptable limits (BIS, 2012; Table 1). As per EC concentrations in the study area, 9% and 14% of samples in pre-monsoon and post-monsoon, respectively, surpassed the BIS acceptable level. Furthermore, according to Richard's classification (Richard, 1954), 5% of pre-monsoon and 2% of post-monsoon samples are in the doubtful category,

and the remaining are under the good to permissible limit (Table 2). TDS is a measure of salinity in groundwater that is important for domestic purposes. The permissible limit (500 mg/L) is exceeded in 20% of the pre-monsoon and 52% of the post-monsoon samples. TDS values were further classified as per Davis and Dewiest (1966) and Freeze and Cherry (1979) (Table 2), signifying that fresh and brackish groundwater samples are found in 95% and 5% of pre-monsoon and 93% and 7% of post-monsoon groundwater samples, respectively. Only 5% of pre-monsoon and 7% of post-monsoon samples are eligible for irrigation, whereas the rest are suitable for all uses. Rock–water interactions generally reduce TDS but may be increased by household wastewater, irrigation return flows, and soil amendments (Adimalla et al., 2020; Raju et al., 2016). The safe drinking water limit for TH is 200 mg/L (BIS, 2012). However, USGS classified samples with more than 300 mg/L as extremely hard (Sawyer & Mc Carty, 1967). The study area's maximum groundwater samples (82% samples in pre-monsoon and 73% in post-monsoon) are in the hard category. In contrast, 9% of pre-monsoon samples and 2% of post-monsoon samples are classified as mild hard, while 9% of pre-monsoon groundwater samples and 25% of post-monsoon groundwater samples are classified as very hard (Table 2). The high TH concentration in groundwater causes arthritis, gallbladders, and urinary stones (Garg et al., 2009).

Further, it produces scales in boilers, well pumps, cooking utensils, water heaters, and washing clothes (Hem, 1991; Todd, 1980) which is a noticeable problem in the study area. All the physicochemical

Table 6 Results of inverse modeling using the means of each group as input

Mineral phases	Model 1		Model 2		Model 3		Model 4		Model 5		Model 6	
	Pre	Post	Pre	Post	Pre	Post	Pre	Post	Pre	Post	Pre	Post
Phase mole transfers Group I to Group II												
Halite	−2.02E-04	−	−1.82E-04	−	−2.02E-04	−	−1.98E-04	−	−9.27E-01	−	−2.31E+00	−
Gypsum	−6.65E-05	−	−6.83E-05	−	−6.65E-05	−	−4.29E-01	−	−8.92E-05	1.03E-04	.	1.03E-04
Anorthite	6.50E-01	−	−	−	5.33E-01	−	−	−	2.54E+00	−	2.31E+00	−
Gibbsite	−4.75E-01	−	−	−	−	−	−	−	.	−	−	−
CO2(g)	5.91E-01	−	−	−	5.33E-01	−	−	−	2.31E+00	−	−	−
Calcite	−5.92E-01	3.23E-04	−3.42E-04	3.23E-04	−5.34E-01	−	−3.14E-04	−	−2.31E+00	−	−4.62E+00	−1.16E-03
Chalcedony	−7.11E-01	−5.37E-04	−	−5.37E-04	−	−1.16E-03	−	−	−	−	−	−
Sylvite	3.78E-05	7.01E-05	3.99E-05	7.01E-05	3.78E-05	1.70E-04	3.82E-05	1.70E-04	9.27E-01	1.70E-04	2.31E+00	1.70E-04
Quartz	−7.11E-01	−5.37E-04	−	−	−	−	−	−1.16E-03	−	−1.16E-03	−4.62E+00	−
Ca-Montmorillonite	−3.54E-01	−	−	−	−	−	−	−	−1.38E+00	−	−	−
Dolomite	−	−	3.68E-05	−	−	−	−	−	−	−	−	−
Kaolinite	−	−	−	−	−5.33E-01	−	−	−	−	−	−	−
Anhydrite	−	−	−	−	−	1.03E-04	4.29E-01	1.03E-04	−	−	−	−
Albite	−	3.41E-04	−	3.41E-04	−	5.66E-04	−	5.66E-04	9.26E-01	5.66E-04	2.31E+00	5.66E-04
K-mica	−	−	−	−	−	−1.88E-04	−	−1.88E-04	−9.27E-01	−1.88E-04	−2.31E+00	−1.88E-04
Illite	−	−1.48E-04	−1.48E-04	−	−	−	−	−	−	−	−	−
Phase mole transfers Group II to Group III												
Halite	−6.49E-04	−1.21E-03	−3.13E-04	−1.21E-03	−3.13E-04	−1.15E-03						
Anhydrite	1.01E-04	−	1.04E-04	−	1.04E-04	−						
Albite	1.03E-03	−	6.93E-04	−	6.93E-04	−						
Calcite	−4.17E-04	−1.46E-03	−1.11E-03	−1.47E-03	−3.72E-04	−2.83E-03						
Dolomite	3.56E-04	−	3.56E-04	−	3.56E-04	3.54E-04						
Chalcedony	−2.06E-03	−	−	−	−9.84E-04	−						
Sylvite	3.37E-04	7.94E-04	−	7.94E-04	−	7.25E-04						
K-mica	−3.43E-04	−7.93E-04	−	−	−	−						
Gypsum	1.01E-04	−1.36E-04	1.04E-04	−1.36E-04	1.04E-04	−1.36E-04						
Quartz	−2.06E-03	−	−	−	−9.84E-04	−						
Anorthite	−	1.19E-03	8.55E-04	1.20E-03	−	2.12E-03						
Ca-Montmorillonite	−	−	−1.03E-03	−	−2.97E-04	−						

Table 6 (continued)

Mineral phases	Phase mole transfers Group I to Group II											
	Model 1		Model 2		Model 3		Model 4		Model 5		Model 6	
	Pre	Post	Pre	Post	Pre	Post	Pre	Post	Pre	Post	Pre	Post
CO2(g)	–	–	9.37E-04	–	–	–	–	–	–	–	–	–
Gibbsite	–	–	–	−1.60E-03	–	−1.46E-03	−6.92E-04	–	–	–	–	–
Kaolinite	–	–	–	–	–	–	−3.46E-04	–	–	–	–	–
Illite	–	–	–	–	–	−1.21E-03	–	–	−4.03E-04	–	–	–
K-feldspar	–	–	–	−7.93E-04	–	–	–	–	–	–	–	–

parameters associated with the EWQI calculation are listed in Table 1. Pre-monsoon EWQI values ranged from 4 to 122. In contrast, post-monsoon EWQI values ranged from 6 to 129 (Fig. 8), implying that the quality of groundwater in the study region varied significantly from excellent (Rank I) to poor (Rank IV). The pH, Mg, and TDS contribution percentages to the EWQI value are maximum, followed by TH, F, and Ca (Fig. 9). NO_3 and Na have moderate contributions, but Cl and SO_4 have low assists, less than 10% contributions. Thus, pH, Mg, and salinity were the key factors in changing the complete groundwater quality. The contribution of quality parameters specified the geogenic control over anthropogenic contribution in the study region. The hardness of the groundwaters may also be justified by Mg's influence from the geogenic weathering processes. Another concerning fact is the contribution of F and Ca to groundwater quality, which may accelerate fluoride concentration balanced by the Ca absorption and suppress fluoride contamination. In particular, the majority of studied groundwaters (approximately 45% in pre-monsoon and 50% in post-monsoon) had excellent EWQI (Rank I) values, with only two samples per monsoon (5%) having EWQI values around 150 and being classified as poor quality (Rank IV) (Fig. 8). In 39% of pre-monsoon and 23% of post-monsoon season samples, the EWQI score ranges between 25 and 50, indicating good water quality (Rank II). Both excellent and good water quality are suitable for drinking and domestic purposes. The remaining samples within the EWQI value of 50 to 100 showed a medium water quality category (Rank III) which is only suitable for domestic purposes. Generally, poor quality to extremely poor water quality is entirely unsuitable for human consumption (Adimalla et al., 2020; Xiao et al., 2021).

Human health risk assessment

In the present study, six samples, each in pre-monsoon and 5 and 8 in post-monsoon, surpass the acceptable limit (Table 1) of NO_3 and F, respectively, as per WHO/BIS guidelines (BIS, 2012; WHO, 2017). Hence, to figure out the extent of health risks, the health hazard index (HHI) is calculated in the current study. The HQ mean concentration of NO_3 in adults is less than one and is almost equal to or greater than 1 in children, indicating that the element constituted low dangers for
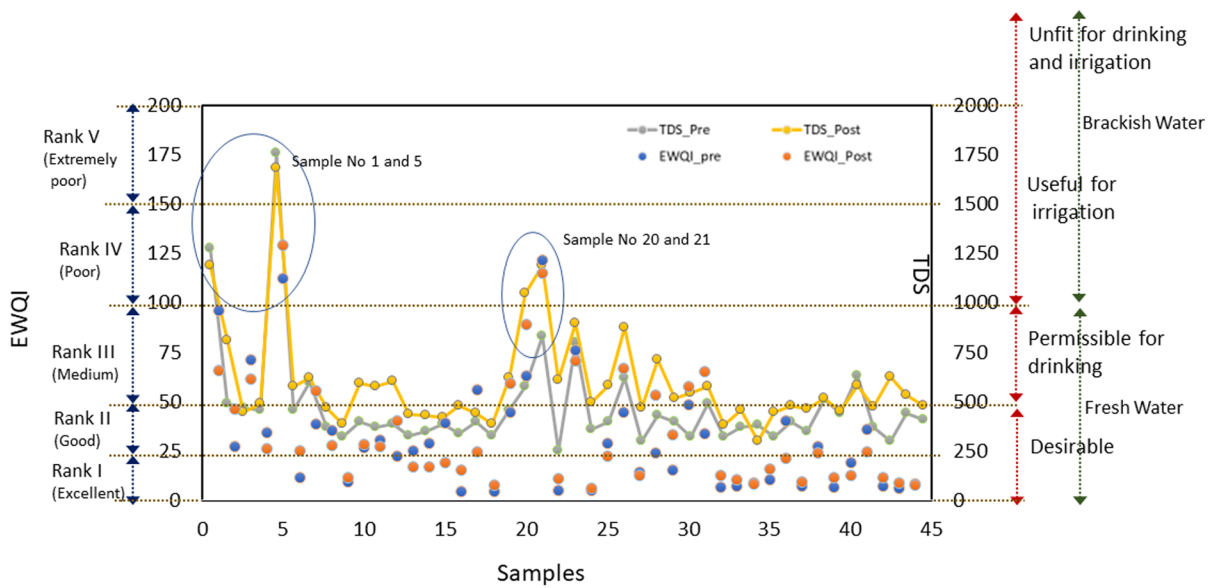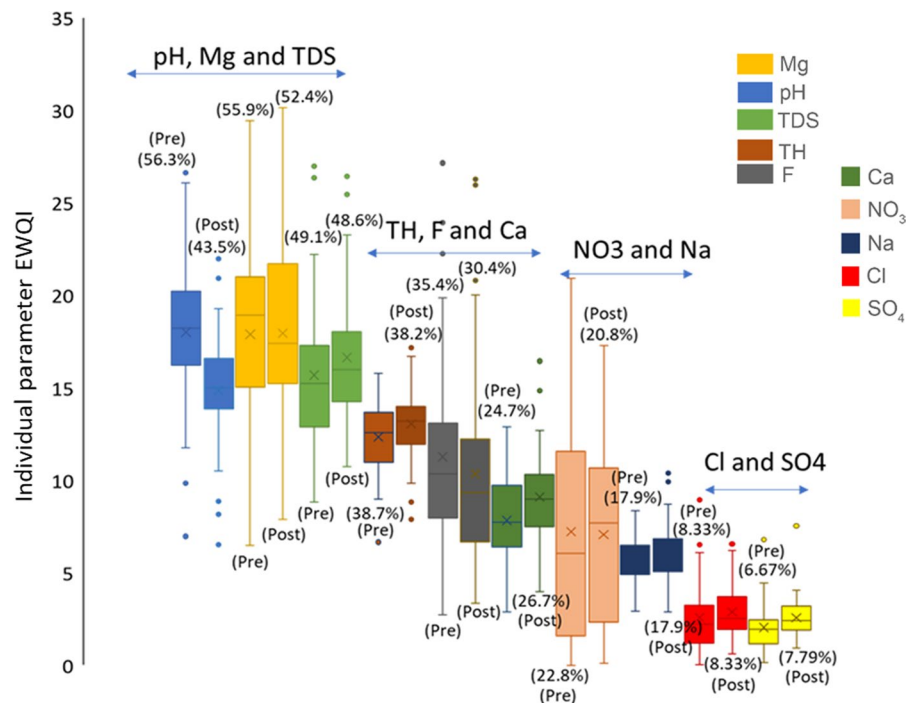
Fig. 8 Graph showing the suitability of groundwater samples for drinking purposes

Fig. 9 Contribution of quality parameters on EWQI values

adults and moderate risks for children for both seasons (Table 7). The HQ values of fluoride exposures indicate greater noncarcinogenic health risks to the child populations, which lessen in adults. The mean HHI is greater than 1 in both age groups (Table 7). Around 93% of groundwaters are above the permissible level for children's noncarcinogenic risk (>1), indicating that they were susceptible to nitrate and fluoride contamination in drinking water. Adult females and males were impacted by 52.3% and 63.6% in pre-monsoon,

Table 7 Calculated human health risk assessment through hazard quotients (HQ) and health hazard index (HHI)

Human health risk (non-carcinogenic)		Hazard quotient fluoride (HQ-F)									
		Min		Max		Mean		% samples < 1		% samples > 1	
		Pre	Post	Pre	Post	Pre	Post	Pre	Post	Pre	Post
Adults	Male	0.45	0.33	2.18	2.68	0.93	1.03	75	61	25	39
	Female	0.54	0.39	2.57	3.17	1.10	1.22	59	39	41	61
Children		0.95	0.69	4.59	5.65	1.95	2.17	2	7	98	93
Hazard quotient nitrate (HQ-N)											
Adults	Male	0.01	0.01	1.38	1.41	0.46	0.54	86	86	14	14
	Female	0.01	0.02	1.63	1.67	0.55	0.64	84	73	16	27
Children		0.01	0.03	2.92	2.98	0.97	1.15	57	43	43	57
Health hazard index (HHI)											
Adults	Male	0.52	0.48	2.74	3.30	1.40	1.86	27	18	72.7	81.8
	Female	0.62	0.57	3.24	3.90	1.65	1.45	16	14	84.1	86.4
Children		1.10	1.02	5.79	6.96	2.95	2.59	0	0	100.0	100.0

respectively, and 65.9% and 79.5% in post-monsoon (Table 7). Post-monsoon season supports more mineral dissolution and thus, may create a higher risk level than pre-monsoon. As per the HHI risk assessment, the order of Children > Females > Males was observed. The leading reason might be the low resistance power of children, followed by females and males. Around the world, several studies on health risks have documented that children are more vulnerable to groundwater contamination (Adimalla et al., 2020; Barzegar et al., 2019; Madhav et al., 2021; Xiao et al., 2021). In general, the noncarcinogenic health risk imposed by nitrate and fluoride will be a source of concern, particularly for children.

The relatively higher nitrate concentrations may be generated by intense agricultural activity, unacceptable sanitary conditions, sewage leachate, and solid waste dumps. Moreover, the deeper aquifers facilitated by sandy soils support nitrate leakage. Hence, high porosity in the alluvial soil of the study area allows rapid infiltration of nitrate but may restrict by clayey soils due to its binding capacity (Raju et al., 2016). On the other hand, observed data show maximum concentration is above 13 mg/L, typically contaminated by anthropogenic activities (Jalali, 2010; Madhav et al., 2021). High NO_3 levels cause health issues such as methemoglobinemia in infants and stomach cancer in adults (Madhav et al., 2021; Raju et al., 2009), whereas excess fluoride concentration introduces endemic fluorosis problems in the human body (Raju et al., 2012).

Micaceous minerals in the sand-clay layers aid the dissolution of fluoride, and subsequently, anthropogenic activities may augment the fluoride content in the groundwater of the study area.

Conclusion

The current study focuses on the hydrogeochemical significance and formation mechanisms of groundwater resources of the Varuna River basin that endured intense instabilities from the human community. Significant seasonal variation was not noticed in the Varuna River basin area. Groundwaters were found to be alkaline, fresh, and hard. The abundance of the major ions is in order of $Na > Ca > Mg > K$ and $HCO_3 > Cl > SO_4 > NO_3 > F$. $Ca-Mg-HCO_3$ appears to be the dominant facies. The study of ratio indices, i.e., Na-normalized molar ratios, Na/Cl, Ca/Mg, and Ca + Mg/TZ+, signifies the presence of silicate weathering, carbonate weathering, and ion exchange processes are responsible for hydrogeochemistry activities in the region. The groundwaters are stable in the kaolinite field due to a well-established groundwater drainage system. An increase in aragonite saturation level from pre-monsoon to post-monsoon specifies that rainfall recharge is the critical factor controlling the ion release. Inverse geochemical modeling

demonstrates the hydrogeochemical changes from Na- HCO_3- Cl (Group I: at recharge area) to Na- Ca- HCO_3 (Group II: transitional area) to Na-Mg-HCO_3 (Group III: discharge area). The changes are mainly due to the dissolution of albite, anorthite, dolomite, gypsum, anhydrite, and sylvite and the precipitation of calcite, gibbsite, Ca-montmorillonite, kaolinite, K-mica, chalcedony, illite, quartz, and halite in the direction of flow. The mixing simulation confirms the match of the compositions of Group II with 50% mixing of each solution in pre-monsoon and mixing of 25% of Group I and 75% of solutions of Group III in the post-monsoon, supporting the mixing between groundwaters in the alluvial plain. Most of the post-monsoon samples exceed the acceptable limit of the pre-monsoon season in terms of TDS (52%), EC (14%), TH (89%), Mg (75%), F (18%), and NO_3 (11%), representing the significant contribution of rainfall in driving the hydrochemical mechanism. The majority of the samples express excellent EWQI (< 25) values (45% in pre-monsoon and 50% in post-monsoon), and only two samples per monsoon (5%) have poor EWQI (100–150). The remaining samples are in between the good to medium quality category. Salinity (TDS), pH, and Mg were the key factors affecting groundwater quality in the study area, indicating geogenic control over anthropogenic contribution. Risk assessment analysis revealed that children are exposed to greater noncarcinogenic health risks than adults concerning nitrate and fluoride concentrations in drinking water. The HHI displays the order of Children > Females > Males, the principal cause of which could be an inadequate resistive capacity of children followed by the females and males. Therefore, limiting anthropogenic activities to prevent contamination should be of primary interest. Eventually, the study aids in improving the area's considerate hydrogeochemical characteristics for a practical multimodal management approach to reflect real-life circumstances better. The findings of this study could lead to new understandings about inferences and optimizations that are locally and socially acceptable for managing groundwater infrastructure at a particular place.

Declarations

References

Adimalla, N., Qian, H., & Li, P. (2020). Entropy water quality index and probabilistic health risk assessment from geochemistry of groundwaters in hard rock terrain of Nanganur County, South India. *Chemie Der Erde, 80*(4), 125544. https://doi.org/10.1016/j.chemer.2019.125544

Amiri, V., Rezaei, M., & Sohrabi, N. (2014). Groundwater quality assessment using entropy weighted water quality index (EWQI) in Lenjanat, Iran. *Environmental Earth Sciences, 72*(9), 3479–3490. https://doi.org/10.1007/s12665-014-3255-0

Appelo, C. A. J. (1994). Cation and proton exchange, pH variations, and carbonate reactions in a freshening aquifer. *Water Resources Research, 30*(10), 2793–2805.

Appelo, C. A. J., & Postma, D. (2005). Geochemistry. *Groundwater and Pollution, 536*, 9781439833544.

Barzegar, R., Asghari Moghaddam, A., Adamowski, J., & Nazemi, A. H. (2019). Assessing the potential origins and human health risks of trace elements in groundwater: A case study in the Khoy plain, Iran. *Environmental Geochemistry and Health, 41*(2), 981–1002. https://doi.org/10.1007/s10653-018-0194-9

Barzegar, R., Asghari Moghaddam, A., Nazemi, A. H., & Adamowski, J. (2018). Evidence for the occurrence of hydrogeochemical processes in the groundwater of Khoy plain, northwestern Iran, using ionic ratios and geochemical modeling. *Environmental Earth Sciences, 77*(16), 1–17.

BIS. (2012). Drinking Water-Specification. Bureau of Indian Standards, New Delhi IS: 10500.

Brown, R. M., McClelland, N. I., Deininger, R. A., & Tozer, R. G. (1970). A water quality index-do we dare. *Water and Sewage Works*, *117*(10).

Chabukdhara, M., Gupta, S. K., Kotecha, Y., & Nema, A. K. (2017). Groundwater quality in Ghaziabad district, Uttar Pradesh, India: multivariate and health risk assessment. *Chemosphere, 179*, 167–178.

CGWB. (2021). National Compilation on Dynamics of Groundwater Resources of India, 2020, 1–401.

Chung, S. Y., Rajendran, R., Senapathi, V., Sekar, S., Ranganathan, P. C., Oh, Y. Y., & Elzain, H. E. (2020). Processes and characteristics of hydrogeochemical variations between unconfined and confined aquifer systems: A case study of the Nakdong River Basin in Busan City, Korea. *Environmental Science and Pollution Research, 27*(9), 10087–10102. https://doi.org/10.1007/s11356-019-07451-6

Dai, Z., Samper, J., & Ritzi, R. (2006). Identifying geochemical processes by inverse modeling of multicomponent reactive transport in the Aquia aquifer. *Geosphere, 2*(4), 210–219. https://doi.org/10.1130/GES00021.1

Davis, S. N., & Wiest, De. (1966). *Hydrogeology*. Wiley.

Dey, S., Shukla, U. K., Mehrishi, P., & Mall, R. K. (2021a). Appraisal of groundwater potentiality of multilayer alluvial aquifers of the Varuna river basin, India, using two concurrent methods of MCDM. In *Environment, Development and Sustainability* (Vol. 23). Springer Netherlands. https://doi.org/10.1007/s10668-021-01400-5

Dey, S., Dey, A. K., & Mall, R. K. (2021b). Modeling long-term groundwater levels by exploring deep bidirectional long short-term memory using hydro-climatic data. *Water Resources Management, 35*(10), 3395–3410. https://doi.org/10.1007/s11269-021-02899-z

Domenico, P. A., & dan Schwartz, F. W. (1990). *Physical and chemical hydrogeology*. Wiley.

Edet, A., & Okereke, C. (2005). Hydrogeological and hydrochemical character of the regolith aquifer, northern Obudu Plateau, southern Nigeria. *Hydrogeology Journal, 13*(2), 391–415.

Fisher, R. S., & Mullican, W. F., III. (1997). Hydrochemical evolution of sodium-sulfate and sodium-chloride groundwater beneath the northern Chihuahuan Desert, Trans-Pecos, Texas, USA. *Hydrogeology Journal, 5*(2), 4–16.

Freeze, R. A., & Cherry, J. A. (1979). *Groundwater*. Prentice-Hall.

Gaillardet, J., Dupré, B., Louvat, P., & Allegre, C. J. (1999). Global silicate weathering and CO2 consumption rates deduced from the chemistry of large rivers. *Chemical Geology, 159*(1–4), 3–30.

Garg, V. K., Suthar, S., Singh, S., Sheoran, A., Garima, M., & Jain, S. (2009). Drinking water quality in villages of southwestern Haryana, India: Assessing human health risks associated with hydrochemistry. *Environmental Geology, 58*(6), 1329–1340. https://doi.org/10.1007/s00254-008-1636-y

Gueroui, Y., Maoui, A., & Touati, A. S. (2015). Hydrochemical and bacteriological investigation in groundwater of the Tamlouka Plain, north-east of Algeria. *Arabian Journal of Geosciences, 8*(5), 2417–2432.

Hem, J. D. (1991) Study and interpretation of the chemical characteristics of natural waters, Book 2254, 3rd edn. Scientific Publishers, Jodhpur

Horton, R. K. (1965). An index number system for rating water quality. *Journal of Water Pollution Control Federation, 37*(3), 300–306.

Jalali, M. (2010). Groundwater geochemistry in the Alisadr, Hamadan, western Iran. *Environmental Monitoring and Assessment, 166*(1–4), 359–369. https://doi.org/10.1007/s10661-009-1007-5

Jandu, A., Malik, A., & Dhull, S. B. (2021). Fluoride and nitrate in groundwater of rural habitations of semi-arid region of northern Rajasthan, India: A hydrogeochemical, multivariate statistical, and human health risk assessment perspective. *Environmental Geochemistry and Health, 43*, 3997–4026. https://doi.org/10.1007/s10653-021-00882-6

Kumar, N., Kumar, D., Kumar, S., Shukla, V., Shukla, P., & Raj, B. (2018). Spatio-temporal variations in hydro-geochemistry of groundwater at rural, urban and industrial areas of Kanpur, India. *Environmental Sustainability, 1*(2), 197–208. https://doi.org/10.1007/s42398-018-0019-x

Li, P., & Wu, J. (2019). Drinking water quality and public health. *Exposure and Health, 11*(2), 73–79.

Liu, J., Peng, Y., Li, C., Gao, Z., & Chen, S. (2021). An investigation into the hydrochemistry, quality and risk to human health of groundwater in the central region of Shandong Province, North China. *Journal of Cleaner Production, 282*, 125416. https://doi.org/10.1016/j.jclepro.2020.125416

Madhav, S., Raju, N. J., & Ahamad, A. (2021). A study of hydrogeochemical processes using integrated geochemical and multivariate statistical methods and health risk assessment of groundwater in Trans-Varuna region, Uttar Pradesh. *Environment, Development and Sustainability, 23*(5), 7480–7508. https://doi.org/10.1007/s10668-020-00928-2

Mall, R. K., Gupta, A., Singh, R., Singh, R. S., & Rathore, L. S. (2006). Water resources and climate change: An Indian perspective. *Current Science*, 1610–1626.

Maskooni, E. K., Naseri-Rad, M., Berndtsson, R., & Nakagawa, K. (2020). Use of heavy metal content and modified water quality index to assess groundwater quality in a semi-arid area. *Water (switzerland), 12*(4), 1–21. https://doi.org/10.3390/W12041115

Mishra, S., Tiwary, D., Ohri, A., & Agnihotri, A. K. (2018). Assessment of groundwater quality using WQI and GIS near the Karsara municipal landfill site, Varanasi, India. *Arabian Journal of Geosciences, 11*(11), 1–9.

Parkhurst, D. L., & Appelo, C. A. J. (2013). Description of input and examples for PHREEQC version 3—A computer program for speciation, batch-reaction, one-dimensional transport, and inverse geochemical calculations. *US Geological Survey Techniques and Methods, 6*(A43), 497.

Patel, P., Raju, N. J., Reddy, B. C. S. R., Suresh, U., Gossel, W., & Wycisk, P. (2016). Geochemical processes and multivariate statistical analysis for the assessment of groundwater quality in the Swarnamukhi River basin, Andhra Pradesh, India. *Environmental Earth Sciences, 75*(7), 1–24. https://doi.org/10.1007/s12665-015-5108-x

Perez, R. J., & Boles, J. R. (2005). An empirically derived kinetic model for albitization of detrital plagioclase. *American Journal of Science, 305*, 312–343.

Piper, A. M. (1944). A graphic procedure in the geochemical interpretation of water-analyses. *Eos, Transactions American Geophysical Union, 25*(6), 914–928.

Raju, J., & RamDey, P. S. (2009). Groundwater quality in the lower Varuna River basin. *Journal of the Geological Society of India, 73*(2), 178–192.

Raju, N. J. (2017). Prevalence of fluorosis in the fluoride enriched groundwater in semi-arid parts of eastern India: Geochemistry and health implications. *Quaternary International, 443*(June), 265–278. https://doi.org/10.1016/j.quaint.2016.05.028

Raju, N. J., Dey, S., Gossel, W., & Wycisk, P. (2012). Fluoride hazard and assessment of groundwater quality in the semiarid Upper Panda River basin, Sonbhadra district, Uttar Pradesh, India. *Hydrological Sciences Journal, 57*(7), 1433–1452. https://doi.org/10.1080/02626667.2012.715748

Raju, N. J., Patel, P., Reddy, B. C. S. R., Suresh, U., & Reddy, T. V. K. (2016). Identifying source and evaluation of hydrogeochemical processes in the hard rock aquifer system: Geostatistical analysis and geochemical modeling techniques. *Environmental Earth Sciences, 75*(16), 1–23. https://doi.org/10.1007/s12665-016-5979-5

Raju, N. J., Shukla, U. K., & Ram, P. (2011). Hydrogeochemistry for the assessment of groundwater quality in Varanasi: A fast-urbanizing center in Uttar Pradesh, India. *Environmental Monitoring and Assessment, 173*(1–4), 279–300. https://doi.org/10.1007/s10661-010-1387-6

Richards, L. (1954). Diagnosis and improvement of saline and alkali soils (USDA. Agriculture handbook, Vol. 60). US Department of Agriculture, Washington DC.

Rimstidt, J. D. (1997). Quartz solubility at low temperatures. *Geochimica Et Cosmochimica Acta, 61*(13), 2553–2558. https://doi.org/10.1016/S0016-7037(97)00103-8

Roy, A., Keesari, T., Mohokar, H., Pant, D., Sinha, U. K., & Mendhekar, G. N. (2020). Geochemical evolution of groundwater in hard-rock aquifers of South India using statistical and modelling techniques. *Hydrological Sciences Journal, 65*(6), 951–968. https://doi.org/10.1080/02626667.2019.1708914

Sami, K. (1992). Recharge mechanisms and geochemical processes in a semi-arid sedimentary basin, Eastern Cape, South Africa. *Journal of Hydrology, 139*(1–4), 27–48.

Sawyer, C. N., & Mc Carty, P. L. (1967). Chemistry for Sanitary Engineers, and classification of naturally soft and naturally hard waters to sources and hardness of their water supplies. *Journal of Hygiene*

Senthilkumar, M., & Elango, L. (2013). Geochemical processes controlling the groundwater quality in lower Palar river basin, southern India. *Journal of Earth System Science, 122*(2), 419–432. https://doi.org/10.1007/s12040-013-0284-0

Shannon, C. E. (1948). A mathematical theory of communication. *The Bell System Technical Journal, 27*(3), 379–423.

Sharif, M. U., Davis, R. K., Steele, K. F., Kim, B., Kresse, T. M., & Fazio, J. A. (2008). Inverse geochemical modeling of groundwater evolution with emphasis on arsenic in the Mississippi River Valley alluvial aquifer, Arkansas (USA). *Journal of Hydrology, 350*(1–2), 41–55. https://doi.org/10.1016/j.jhydrol.2007.11.027

Shukla, U. K., Srivastava, P., & Singh, I. B. (2012). Migration of the Ganga River and development of cliffs in the Varanasi region, India during the late Quaternary: Role of active tectonics. *Geomorphology, 171*, 101–113.

Singh, A. K., Tewary, B. K., & Sinha, A. (2011). Hydrochemistry and quality assessment of groundwater in part of NOIDA metropolitan city, Uttar Pradesh. *Journal of the Geological Society of India, 78*(6), 523–540.

Singh, I. B. (1996). Geological evolution of Ganga Plain—An overview. *Journal of the Palaeontological Society of India, 41*, 99–137.

Singh, S., Raju, N. J., Gossel, W., & Wycisk, P. (2016). Assessment of pollution potential of leachate from the municipal solid waste disposal site and its impact on groundwater quality, Varanasi environs, India. *Arabian Journal of Geosciences, 9*(2), 1–12.

Singh, S., Raju, N. J., & Ramakrishna, C. (2015). Evaluation of groundwater quality and its suitability for domestic and irrigation use in parts of the Chandauli-Varanasi region, Uttar Pradesh, India. *Journal of Water Resource and Protection, 7*(7), 572.

Subba Rao, N., Sunitha, B., Adimalla, N., & Chaudhary, M. (2020). Quality criteria for groundwater use from a rural part of Wanaparthy District, Telangana State, India, through ionic spatial distribution (ISD), entropy water quality index (EWQI) and principal component analysis (PCA). *Environmental Geochemistry and Health, 42*(2), 579–599. https://doi.org/10.1007/s10653-019-00393-5

Timoshenkova, A. N., Pasechnik, E. Y., & Tokarenko, O. G. (2014). Equilibrium of groundwater with carbonate minerals of the water-bearing rocks under anthropogenic impact (by the example of Kishinev, Moldova). *IOP Conference Series: Earth and Environmental Science*. https://doi.org/10.1088/1755-1315/21/1/012024

Todd, D. K., & Mays, L. W. (1980). *Groundwater hydrology* (p. 535). Wiley.

Tong, S., Li, H., Tudi, M., Yuan, X., & Yang, L. (2021). Comparison of characteristics, water quality and health risk assessment of trace elements in surface water and groundwater in China. *Ecotoxicology and Environmental Safety, 219*, 112283. https://doi.org/10.1016/j.ecoenv.2021.112283

Tyagi, S., & Sarma, K. (2020). Qualitative assessment, geochemical characterization and corrosion-scaling potential of groundwater resources in Ghaziabad district of Uttar Pradesh, India. *Groundwater for sustainable development, 10*, 100370.

UNICEF, & WHO. (2004). *Meeting the MDG derinking water and sanitation target. A Mid-Term Assessment of Progress*.

USEPA (2022). *Regional Screening Levels (RSLs)—Generic Tables as of: May 2022,* from https://www.epa.gov/risk/regional-screening-levels-rsls-generic-table.

Wernberg, T. (1998). Transport par l'eau souterraine de composés multiples avec prise en compte des équilibres chimiques et des cinétiques: Développement et évaluation du modèle. *Hydrological Sciences Journal, 43*(2), 299–317. https://doi.org/10.1080/02626669809492123

WHO. (2017). *Guidelines for drinking-water quality*, fourth ed. incorporating the first addendum. Geneva.

Xiao, Y., Liu, K., Yan, H., Zhou, B., Huang, X., Hao, Q., Zhang, Y., Zhang, Y., Liao, X., & Yin, S. (2021). Hydrogeochemical constraints on groundwater resource sustainable development in the arid Golmud alluvial fan plain on Tibetan plateau. *Environmental Earth Sciences, 80*(22), 1–17. https://doi.org/10.1007/s12665-021-10076-z

Zhang, H., Xu, G., Zhan, H., Chen, X., Liu, M., & Wang, M. (2020). Identification of hydrogeochemical processes and transport paths of a multi-aquifer system in closed mining regions. *Journal of Hydrology, 589*, 125344. https://doi.org/10.1016/j.jhydrol.2020.125344